Contribution of the cold sector of extratropical cyclones to mean state features over the Gulf Stream in winter

Benoît Vannière [a*] Arnaud Czaja [a*] Helen F Dacre [b*]

[a] *Physics Department, Imperial College London, London, United-Kingdom,*

[b] *Department of Meteorology, University of Reading, Reading, United-Kingdom*

[*]Correspondence to: B. Vannière, Imperial College, Department of Physics, Space and Atmospheric Physics Group,Huxley Building, Room 716, London SW7 2AZ. email: b.vanniere@imperial.ac.uk

Recent studies have shown that midlatitude air-sea interactions are strongly modulated by synoptic variability. The present study investigates how air-sea interactions over the Gulf-Stream sea surface temperature (SST) front vary in different synoptic regimes. We focus more particularly on the variation of three atmospheric mean state features which are colocated with the SST front in winter : enhanced ascent and precipitation on the south warm side of the SST front and the enhanced low-level baroclinicity at the entrance of the storm track. These three fields are partitioned depending on whether they occur in the cold sector of extratropical cyclones or in any other synoptic regime. The analysis is based on ERA-interim winter data covering the period 1979-2012. Results are twofold. (i) Cold sector precipitation is confined within a 5° band following the SST front and reaches 2 mm.day^{-1} whereas precipitation occurring outside the cold sector forms a broader spatial pattern. The same partitioning applied to vertical winds show that the ascent on the warm side of the Gulf Stream is not a feature of the cold sector and that it cannot be directly related to the enhanced precipitation as suggested by previous studies. These results shows that a significant part of the anchoring effect of the SST front on precipitation is via the cold sector but that the observed colocation of ascent and precipitation highlighted in previous studies is not causal and reflect two different mechanisms. (ii) The surface heat fluxes and convection occurring in the cold sector restore the low-level thermal gradient, within 48 hours of a cyclone passage such that low-level baroclinicity remains largely unchanged after the passage of a storm. This "cold path mechanism" opens new avenues to understand how SST forces climate variability in the midlatitudes.

Key Words: Cold Sector; Extratropical cyclone; Gulf-Stream; Air-Sea interactions; North Atlantic climate

1. Introduction

During boreal winter, a sharp sea surface temperature (SST) front develops between the warm waters transported by the Gulf Stream and the cold waters of the continental shelf. Observations and numerical experiments have provided several lines of evidence of a climatological impact of the Gulf Stream SST front on the troposphere. For instance, satellite data at high resolution revealed the tight relationship between the SST front and mesoscale features of the low-level atmosphere, such as the curl and divergence of wind stress (Chelton *et al.* 2004) and cloud cover (Small *et al.* 2008). Atmosphere only experiments further suggested the anchoring effect of the SST front on precipitation and vertical wind (Minobe *et al.* 2008). Finally, sensitivity experiments showed that the presence of the SST front leads to an enhancement of low-level baroclinicity and eddy kinetic energy further downstream (Nakamura *et al.* 2008; Brayshaw *et al.* 2009). However, there has been recent claims that, despite the permanent presence of the SST front, air-sea interactions over the Gulf Stream are strongly modulated by synoptic activity (2 to 10 day atmospheric variability) in winter (Hand *et al.* 2014; Liu *et al.* 2014; Parfitt and Czaja 2015; Vanniere *et al.* 2015). Thus, further progress in understanding the climatological anchoring effect of the SST front requires us to investigate how air-sea interactions behave under different synoptic regimes. In the present study, we will use recently developed tools (Vannière *et al.* 2015) to partition the processes of the Gulf Stream region according to the synoptic regime in which they occur, with a special focus on cold sector situations. Following the American Meteorological Society, we define the cold sector as the area within the circulation of an extratropical cyclone, behind the cold front, where cold air advection occurs. In the remaining part of the introduction, we review the proposed mechanisms controlling the interaction of the SST front with (i) tropospheric circulation and precipitation and (ii) baroclinicity, and how this interaction is modulated at synoptic time scales.

Minobe *et al.* (2008) proposed a climatological pathway by which the Gulf Stream SST front affects tropospheric ascent and precipitation. They suggest that the pressure in the marine atmospheric boundary layer adjusts to the SST front, by generating surface wind convergence and ascent on the warm side of the SST front which anchors a band of precipitation. This is depicted in figure 1, where the climatological mean (1979-2010) of vertical wind in pressure coordinates (ω) from ERA interim forms a band of enhanced ascent on the warm edge of the SST front (figure 1(b)), reaching 200hPa (figure 1(a)). The mechanism proposed by Minobe *et al.* (2008) combines all the mean climatological features of this region with simplicity. But it is not obvious how it connects to the day-to-day synoptic activity in the region. Indeed, if we analyse the median, rather than the mean, median vertical winds feature a subsiding regime on the warm edge of the SST front, emphasising how sensitive ascent is to synoptic activity (figure 1(c,d)).

In a numerical case study of an extratropical cyclone forced respectively by observed and smoothed SSTs, Vanniere *et al.* (2015) showed that the anchoring effect of the SST front was mostly related to convective precipitation in the cold sector. The question thus arises; to what extent cold sector convective precipitation contributes to the mean climatological precipitation over the Gulf Stream. In a composite of the top 5% of strongest storms, Vannière *et al.* (2015) showed that a significant part of precipitation, albeit weaker than in the warm conveyor belt (WCB), occurred in the cold sector. As 95% of precipitation in the storm track region is produced by extratropical cyclones (Hawcroft *et al.* 2012), the cold sector convective precipitation could have a non negligible contribution to climatological precipitation in the Western North Atlantic. A mechanism acting to anchor the cold sector precipitation would have the advantage of explaining the strong seasonality of the observed Gulf Stream rain band. Furthermore it would also explain why the anomalous precipitation that extends far offshore along the SST front during winter remains confined to the North American coast in summer (Minobe *et al.* 2010): there is no cold air outbreak in summer and thus lesser anchoring than in winter. Moreover, by further analysing Minobe *et al.* (2008) experiments, (Kuwano-Yoshida *et al.* 2010) found that although the anomalous vertical wind associated with the SST front tends to reach the tropopause during summer, it remains confined to the lower half of the troposphere during winter, possibly due to the more stratified troposphere in winter. Finally, a role of the cold sector would

also be consistent with another finding of Kuwano-Yoshida *et al.* (2010) who showed that the anomalous precipitation associated with the SST front was exclusively convective (their AGCM has half a degree horizontal resolution), whereas one would expect the warm sector to set large scale precipitation anomalies.

The effect of the SST front is not only to anchor mesoscale features such as vertical wind and precipitation, but also to favor the development of baroclinic cyclones by causing high low-level baroclinicity. The role of midlatitude SST fronts in anchoring a downstream storm track has been demonstrated by Nakamura *et al.* (2008) in an aqua-planet experiment. Even though land-sea contrast and topography have been shown to play a dominant role in enhancing low-level baroclinicity over the North Atlantic basin Brayshaw *et al.* (2009), the Gulf Stream SST front may also contribute to it, too.

There has been much debate in the literature as to whether sensible heat flux (Hotta and Nakamura 2011) or latent heat release (Hoskins and Valdes 1990; Papritz and Spengler 2015) is the main mechanism enhancing baroclinicity. Extratropical cyclones erode the thermal gradients upon which they develop, so that the existence of an organised storm track is conditioned to a mechanism restoring baroclinicity. The idea of intermittent bursts of heat transport with a subsequent restoring of potential energy underpins the non-linear oscillator model proposed by Ambaum and Novak (2014). The time scale of the restoring processes determines the shape of the oscillation. Ambaum and Novak (2014) attempted to evaluate this time scale based on ERA interim composites of baroclinicity before and after a maximum of surface heat fluxes in the Western North Atlantic. A large part of the low-level baroclinicity was found to be restored in the 24h following the heat transport maximum. A similar time scale was found by Nonaka *et al.* (2009) in the Antarctic Polar Front Zone for a composite of 8 cold air outbreaks, a situation where cold and dry continental air is advected over warmer waters. This rapid restoring suggests that the mechanism might occur within or in association with the eroding process (in the extratropical cyclone). Using a baroclinic wave model, Hoskins and Valdes (1990) proposed that latent heat release in the WCB of the storm itself could modify mid-troposphere baroclinicity (as defined by the Eady growth rate) and favor baroclinic cyclogenesis. Conversely, the strong surface sensible heat fluxes of the cold sector could act to restore low-level baroclinicity (Nakamura *et al.* 2008) via baroclinic adjustment. A recent study by Papritz and Spengler (2015) calculated a full budget of processes setting the slope of the isentropic surfaces in the atmosphere. The displacement of isentropic surfaces by growing baroclinic disturbances was found to reduce the slope of isentropic surfaces. On the contrary, diabatic processes were shown to increase the slope. Interestingly, Papritz and Spengler (2015) showed that the diabatic production of isentropic slope in the low troposphere was associated 80% of time with cold air outbreaks, suggesting a role for the cold sector in restoring baroclinicity.

In summary, the goal of this study is to composite precipitation occurring in the cold sector sectors of extratropical cyclones and to quantify the role of the cold sector precipitation in shaping the region of ascent and high baroclinicity along the SST front. The article is organised as follows: data and methods are presented in section 2, results in section 3 and discussion in section 4 and conclusion is provided in section 5.

2. Data and method

2.1. Reanalysis data

The ERA interim dataset is a reanalysis of the global atmosphere covering the period since 1979, and continuously updated in real time Berrisford *et al.* (2009). In this study, we used December to February data over the period 1979-2012. It uses 60 levels in the vertical and a spectral truncation of T255 (the reduced Gaussian grid has a 79 km spacing for surface and other grid-point fields). The data used in this paper has a resolution of 1.5°. The fields are on the native pressure levels.

ERA-interim includes a moist boundary-layer scheme based on eddy diffusion combined with mass-flux transport (Köhler 2005; Köhler *et al.* 2011). The mixed-layer height is determined using an entraining parcel, selecting the top of stratocumulus, or cloud base in shallow convection situations.

In this paper, large scale and convective precipitation is based on forecast data initialised at 1200 UTC and accumulated over

3 hours. Hawcroft *et al.* (2012) showed that the magnitude of precipitation rate was not reliable for the first 3-9 hours of the forecast due to the spin-up effects, whereas the pattern was not significantly altered. As a result, the sensitivity of the decomposition to the leadtime used will be discussed in section 4. The distinction between convective and large scale precipitation is often argued to be misleading, as the split is essentially determined by the model resolution. Nevertheless, we will use this distinction because it can help infer the physical processes leading to precipitation (e.g., Kuwano-Yoshida *et al.* (2010)).

2.2. *Cold sector indicator*

To identify the cold sector, we use an indicator combining PV at 975mb and sensible heat flux (Vannière *et al.* 2015). Such an indicator was tested in a composite of 57 storms corresponding to the 5% strongest storms in the Gulf Stream region, and it allowed a systematic and accurate detection of cold sector precipitation and subsidence (see a detailed discussion in Vannière *et al.* (2015)).

Here, locations where a given grid cell x at a given time t has negative PV at 975 mb and upward surface sensible heat flux above the threshold value 50 $W.m^{-2}$ is defined as being in the cold sector and noted CS. The notation $\overline{CS}$ corresponds to all the other locations. The indicator of the cold sector is defined as follows :

$$1_{CS}(x,t) = \begin{cases} 1 & \text{if } (x,t) \in CS, \\ 0 & \text{if } (x,t) \notin CS, \end{cases}$$

The contribution to the climatological mean (μ) of a variable (F) can be expressed as the mean under a given synoptic situation (m) times the frequency of this synoptic situation (P). This can be written as follows :

$$\mu_{CS}(F) = m_{CS}(F) \times P(1_{CS})$$

$$\mu_{\overline{CS}}(F) = m_{\overline{CS}}(F) \times P(1_{\overline{CS}})$$

In the case of precipitation, we want to achieve a partitioning of the total precipitation budget and therefore μ is calculated. Note that μ does not reflect the atmospheric state of the atmosphere in a cold sector situation, but rather the contribution of the cold sector to this mean. To estimate the mean atmospheric state in a cold sector, the mean of cold sector ($m_{CS}(F)$) and outside the cold sector ($m_{\overline{CS}}(F)$) are used.

3. Results

3.1. *Case study*

We first analyse a case study of a storm which passed over the Gulf Stream region on 27 January 1985 to illustrate the strong interaction between the cold sector precipitation and the SST front. Figure 2a shows total precipitation on 27 January at 0000 UTC, when the extratropical cyclone reaches its maximum intensity. One can recognise the classical τ-shape of the WCB with its lower branch wrapping cyclonically around the low pressure center. The WCB is characterised by heavy precipitation rates up to 40 mm.day^{-1}. Another band of precipitation, is observed west of the WCB and lies parallel to the Gulf Stream SST front (black contours). This band of precipitation is located in the cold sector (regions where the cold sector indicator is positive are enclosed in red contours). Figure 2(b) shows concomitant upward motion at 700 mb characteristic of the Warm Conveyor Belt. In the cold sector, a dipole of ascent/subsidence centred on the SST front is observed. Along the North American coast, neither convection nor upward motion are observed, as air parcels need to accumulate enough heat and moisture for convection to develop (Vanniere *et al.* 2015). All these results are consistent with those found in Vanniere *et al.* (2015) and suggest that cold sector convection can strongly interact with the SST front in ERA interim data.

In Fig. 3 equivalent potential temperature at 950 mb, which characterise warm and cold sector air masses, is represented. On 26 January (Fig. 3 (a)), a tongue of warm air starts developing and crosses the SST front between 60°W and 50°W. On 27 January the warm sector has propagated eastward and the warm tongue has further developed. West of the warm tongue however, the tongue of cold air is less marked, as the cold advection is strongly damped by surface turbulent fluxes (Fig. 3 (b)). On 28 January, isotherms are oriented in the same direction as the SST front again and on 29 Janurary the temperature south of the SST front reaches same value as on 26 January. This sequence suggests that low-level temperature gradients in the atmosphere are restored rapidly

by the strong surface fluxes and convection in the cold sector. In a similar way, we expect low-level baroclinicity to be restored rapidly after the passage of the extratropical cyclone.

A good measure of baroclinicity is the Eady growth rate Hoskins and Valdes (1990), which is calculated as follows:

$$\sigma = 0.31 \frac{f}{N} \left| \frac{\partial u}{\partial Z} \right| \quad (1)$$

where the Coriolis parameter, $f = 2\Omega sin\phi$, Ω, the rotation rate of the Earth, g, the gravity, and ϕ, the latitude and the Brunt-Vaisaila frequency, $N = g\partial \ln\theta/\partial Z$, θ is potential temperature and Z is geopotential. The height derivatives are evaluated between levels 850 and 700 mb. Classically, the Eady parameter is calculated using climatological fields. More recently, however, time series of the Eady parameter have been composited around time maxima of eddy heat transport to describe the reduction of baroclinicity by atmospheric disturbances and its subsequent restoration Ambaum and Novak (2014). Since such composites will be reproduced in section 3.4, it is useful to assess first the evolution of the Eady parameter during the course of a single extratropical cyclone.

The instantaneous value of the Eady growth rate is overlaid in blue contours on Fig. 3. As seen on Fig. 3(a) and (b), the Eady parameter tends to be high along the warm front of the extratropical cyclone. In the region of warm advection itself baroclinicity is low, which is consistent with the general idea that horizontal advection destroys temperature gradients and reduces baroclinicity. Baroclinicity increases again in the cold sector between 27 and 29 January and the region of high baroclinicity, initially confined to the North American coast, develops eastward. From 28 January, the highest baroclinicity values are colocated with the highest SST gradient.

We now evaluate the evolution of low-level baroclinicity around the maxima of the eddy heat transport averaged over the domain [80°W-30°W,30°N-50°N]. This diagnostic is inspired by Ambaum and Novak (2014) but here the tendency of baroclinicity is shown instead of baroclinicity itself. The eddy heat transport is calculated at 850 mb and a high-pass filter with a 10-day cutoff is applied to v and T in order to obtain synoptic variability. Baroclinicity decreases over the domain before the maximum of eddy heat flux (green and black curves, respectively, on Fig. 4(a)) and increases immediately after. The contributions of CS (blue line) and $\overline{CS}$ (red line) to the tendency of baroclinicity are also shown on Fig. 4 (a). The reduction of baroclinicity occurs in $\overline{CS}$ in phase with the maximum of eddy heat flux and most likely due to horizontal advection. Conversely, the increase of baroclinicity occurs in CS, after the maximum of the eddy heat flux, when surface turbulent heat fluxes in the cold sector are the strongest Fig. 4 (c). This sequence of events supports the idea that for this particular extratropical cyclone, the strong surface heat fluxes and convection in the cold sector played a key role in restoring low-level baroclinicity.

In the following subsections, we evaluate the distribution and the amount of precipitation, vertical motion and baroclinicity occurring in the cold sector and outside the cold sector in the climatology.

3.2. *Precipitation*

The ERA-interim climatological mean precipitation, shown on Fig. 5 (a), was partitioned between the cold sector (CS) and the remainder of synoptic situations, referred to as non cold sector situations ($\overline{CS}$) hereafter, in Fig. 5 (b) and (c), respectively. The colorbars are different in each panel in order to highlight the difference in meridional extent of the precipitation pattern. In the domain [85°W-25°W,25°N-55°N] (referred to as "Gulf Stream region" hereafter) CS precipitation represents 11.3% of the total precipitation. Despite representing only a small fraction of the total precipitation, CS spatial distribution may influence the pattern of total precipitation. Indeed, precipitation occurring in CS forms a band following the line of the SST front and reaches up to 2 mm.day^{-1} on the warm side of the SST front, i.e. south of the maximum SST gradient. In contrast, precipitation occurring in $\overline{CS}$ forms a more widespread pattern over the SST front. The latter peaks south of the SST front at 37°N and has an amplitude of 5 mm.day^{-1}. In order to measure the difference of spatial spread between precipitation occurring in CS and $\overline{CS}$, we compare the area where mean precipitation exceeds 50% of the maximum value. This area is given as a fraction of the Gulf Stream region (see definition above) and is called ρ. The value of ρ was found to be 0.18 and 0.50 in CS and $\overline{CS}$, respectively, confirming the larger confinement of CS precipitation.

We further decompose the precipitation into convective and large scale components (Supplementary figure). The band of precipitation in the cold sector comprises 70% convective precipitation. The remaining 30% forms a band of large scale precipitation also following the SST front. However, the large scale precipitation occurring in the cold sector must be interpreted with some caution. Indeed as described by Vannière *et al.* (2015), the cold sector indicator can capture some large scale precipitation from the WCB due to the vertically sloped nature of the cold front. The precipitation in $\overline{CS}$ splits into convective precipitation on the warm side of the front and large scale precipitation north of it, corresponding to the entrance of the warm conveyor belt and to the upper branch of the WCB respectively. To test whether an incorrect attribution of large scale precipitation to the cold sector could change our conclusions on the different spread of precipitation, ρ was calculated again for convective precipitation in the cold sector only and for the rest of precipitation. The new values of ρ are now 0.22 and 0.50 respectively, so that our conclusions are not affected by this caveat.

3.3. *Vertical wind*

The cold sector mask is now applied to ERA interim vertical wind at 700 mb. The time mean vertical wind (figure 6 (a)) is the result of a balance between the contributions of CS (b), dominated by subsidence, and $\overline{CS}$ (c). The two contributions largely cancel out, as their sum is one order of magnitude less than each taken separately. It is clear that in $\overline{CS}$, ascent is strongest on the warm side of the SST front. This is explained by the strong adiabatic ascent along the sloped isentropic surfaces originating from the SST front (Parfitt and Czaja 2015). Interestingly, the cold sector subsidence is the weakest south of the front. We also find that 25% of the time cold sector air is ascending on the warm side of the front (not shown). This leads us to evaluate vertical wind in the more specific situation where convection occurs in the cold sector. In figure 6 (d) we composite cold sector situations with convective precipitation greater than 5 mm.day^{-1}. In those situations, ascent dominates on the warm edge of the SST front and represents 20% of the total vertical ascent (compare Fig. 6 (a) and (d)). This cold sector ascent is consistent with the circulation cell crossing the SST front described in the cold sector of an extratropical cyclone passing over the Gulf Stream in Vannière *et al.* (2015).

In conclusion, the enhancement of mean ascent and precipitation on the warm side of the SST front occurs through two different synoptic regimes, respectively the cold and non cold sector situations. It is likely that the strong ascent on the warm side of the front is mainly set by the ascending motion in WCBs. However, this cannot be definitively stated as warm sector is only one of several synoptic situations contained in the non cold sector composite. Cold sector precipitation is associated with ascent but this ascent represents only a small fraction of the total and cannot be viewed as the primary contribution setting its banded pattern.

3.4. *Baroclinicity*

As section 3.2 showed that cold sector convection was favoured on the warm side of the SST front at the expense of the cold side, it is possible that convection together with surface heat fluxes contribute to the restoration of low-level baroclinicity in the wake of extratropical cyclones.

Figure 7 shows the mean baroclinicity at 775 mb (a), its mean value in CS (b) and $\overline{CS}$ (c) and the percentage change between CS and $\overline{CS}$ (d). The mean Eady growth reaches its highest values over the maximum of the SST gradient. The same colocation happens when the subset of CS situations is considered. In $\overline{CS}$, however, the maximum values occur slightly north of the SST front, which could be due to the advection of the warm front of extratropical cyclones by southerly winds in the warm sector (which showed in section 3.1 that the warm front was detected by the Eady growth rate). South of the SST front, baroclinicity is larger in CS than for the remaining situations by an excess of 10 to 30 % (Figure 7 (d)). These results are compatible with a restoring of high baroclinicity over the highest SST gradient via the cold sector.

To ascertain the scenario that baroclinicity is restored in the cold sector, we reproduce the diagnostic presented in Fig. 4, compositing the tendency of low-level baroclinicity around the time maxima of eddy heat transport. The time series of baroclinicity tendency and eddy heat flux are obtained as in section 3.1. Results are presented in Fig. 8 (a). As in the case

study (section 3.1), there is a strong decrease and increase of low-level baroclinicity (see green curve) before and after a burst of eddy heat flux (black curve). The contributions of CS (blue line) and $\overline{CS}$ (red line) to the baroclinicity tendency are also presented in Fig. 8 (a). At all time, the baroclinicity tendency is negative in $\overline{CS}$ and positive in CS, showing the preferential role of the cold sector to restore baroclinicity. Around the maximum of eddy heat flux, variations of baroclinicity are interpreted as follows. When the eddy heat flux reaches its maximum, the horizontal mixing induced by the extratropical cyclone reduces temperature gradients and therefore the mean baroclinicity in the domain. This reduction occurs primarily due to horizontal advection outside the cold-sector ($\overline{CS}$). Note that the contribution of $\overline{CS}$ to total surface heat fluxes does not vary much before and after the passage and is less than 70 $W.m^{-2}$ at all time (see red curve in figure 8 (b)). As the cyclone moves further eastward, a large part of the domain is in the cold sector, where strong surface turbulent fluxes occur, 160 $W.m^{-2}$ on average (see figure 8 (b)). The differential of turbulent fluxes on both sides of the SST front leads to an increase of cold sector baroclinicity (blue curve on Fig. 8 (a)). After 48 hours, the net baroclinicity of the domain is back to its value before the passage of the storm (not shown). In conclusion, baroclinicity evolves in the composite in a similar manner as in the case study presented in section 3.1.

We further investigate whether the restoration of baroclinicity in the cold sector is caused by a change in stability (N) or in wind shear ($\left|\frac{\partial u}{\partial Z}\right|$). At least two mechanisms can be considered : a decrease of stability in response to the strong surface turbulent fluxes or an increase of wind shear ($\left|\frac{\partial u}{\partial Z}\right|$), related to horizontal temperature gradients by the thermal wind balance, in response to the differential heating on both sides of the SST front. The respective role of wind shear and stability is evaluated by replacing their climatological values in the calculation of σ. We find that wind shear and stratification have opposite effects: the strong wind shear increases baroclinicity in CS in comparison to $\overline{CS}$, whereas the enhanced stability above the boundary layer tends to decrease it slightly (not shown). The higher stability in the cold sector is explained by the strong stratification of the free troposphere above the boundary layer.

4. Discussion

As a quantitative partitioning is undertaken in this study, it seems important to assess the sensitivity of our results to the methodology.

First, the reported biases in ERA interim precipitation associated to the model spin-up may alter the proportion of precipitation occurring in the cold sector. To test whether our conclusions are sensitive to the spin-up, we carried out the same partitioning as in section 3.2 but now evaluating precipitation at a 9-hour lead time instead of 3-hour as before. The cold sector indicator is based on the analysed PV at 975 mb and 1800 UTC and forecasted surface sensible heat fluxes. In order to be consistent with the method used in subsection 3.2, precipitation and surface sensible heat fluxes are evaluated over the three hours following 1800 UTC. To do so, we use forecast data initialised at 1200 UTC and take the difference of the accumulated fields over 6 and 9 hours. The proportion of precipitation falling in the cold sector, now 12.3%, is not significantly different from previously found using a 3-hour lead time, namely 11.3% (see subsection 3.2). Thus the choice of the lead time does not seem to have much effect on the proportion of cold sector precipitation.

Secondly, choosing multiple criteria to define the cold sector mask is always a trade-off between accuracy and systematicity as discussed in Vannière *et al.* (2015). Moreover, the ability of a given criterium to detect CS may differ spatially. For example, surface sensible heat flux is on average larger on the warm edge of the SST front, where it passes more often the threshold value defining CS. This might reinforce the contrast between the north and south edge of the SST front and amplify the band of precipitation. We tested how the addition of the criterium based on sensible heat flux in CS diminishes the proportion of cold sector precipitation detected. Therefore, we recomputed the mask with the PV criterium only : the proportion of precipitation falling in the cold sector is now 18.2%, and must be compared to 11.3% when both PV and surface sensible heat flux are used. We expect the true amount of precipitation in the cold sector to lie between those two values.

Finally, we discuss our conclusions on the role of the cold sector in restoring low-level baroclinicity. This conclusion relies

both on the fact that CS contributes to the restoration of baroclinicity and that we did not find a significant difference of baroclinicity a few days before and after the maximum of eddy heat flux. We note that this difference was marginal in Ambaum and Novak (2014) and we found that it is sensitive to the criteria retained to build the composite. Hence, we do not deny that other physical processes may participate in the restoration of baroclinicity on time scale of a few days as suggested by Ambaum and Novak (2014), but results suggest that the main source of restoration of baroclinicity occurs in the cold sector of the storms itself. This result is consistent with Nonaka *et al.* (2009) who showed that along SST fronts in the southern Indian Ocean, low-level horizontal temperature gradients were restored in 24 hours after the passage of a storm.

5. Summary and conclusions

The cold sector of extratropical storms in ERA interim data is found to be dominated by convective precipitation, tightly linked to the Gulf Stream SST front. During convective events, a dipole of ascent/subsidence at 700mb, centred on the SST front, is observed. To assess the significance of cold sector contribution to climatological precipitation, ERA interim precipitation has been partitioned depending on whether it occurs in the cold sector of extratropical storms or in the remainder of synoptic situations. A PV indicator described in Vannière *et al.* (2015) has been used for the partitioning. We find that non cold sector precipitation forms a broad pattern peaking on the warm side of the SST front. This pattern resembles the distribution of warm conveyor frequency presented in Pfahl *et al.* (2014). On the contrary, cold sector precipitation is confined within 5° in a sharp band following the Gulf-Stream SST front. These results suggest that a significant part of the anchoring effect of the SST front on precipitation is via the cold sector. As the observed band of precipitation has often been associated with vertical ascent on the warm edge of the front, the PV indicator was applied to evaluate vertical wind in the cold and non cold sectors respectively. The contributions from these two parts of the storm largely cancel out to set the mean pattern.

These results demonstrate the importance of synoptic variability in controlling how the sea surface connects to the troposphere. Interestingly, cold sector precipitation has the same amplitude as the reduction of precipitation in response to a smoothing of the SST gradients (Minobe *et al.* 2008). It is thus plausible that the response of the SST front smoothing occurs mostly in the cold sector. In contrast, the strong ascent on the warm side of the SST front can not be attributed solely to the cold sector, as the stronger vertical wind south of the SST front is also seen outside the cold sector. Hence no direct causal link between ascent and precipitation on the warm side of the Gulf Stream can be made. It is nevertheless of interest to emphasise that an indirect link between precipitation and vertical wind still exists : convective adjustment leads to a steepening of isentropic surfaces in the cold sector which can generate stronger adiabatic ascent in the warm sector of subsequent storms.

This study also highlights the contribution of cold sector processes in setting low-level baroclinicity and preconditioning the atmosphere for the development of subsequent storms. We have tested the role of differential surface turbulent fluxes and convective activity on both sides of the SST front in restoring baroclinicity in the cold sector of storms. The cold sector mask was applied to partition low-level baroclinicity tendency and surface heat fluxes for a composite of strongest eddy heat fluxes. Baroclinicity increase was shown to occur in the cold sector after the maximum of eddy heat flux and concurrently with strong surface heat fluxes. Once restored, baroclinicity increases passively in the non cold sector as the cold sector moves away. In the entire domain, baroclinicity is restored after approximately two days.

This finding supports the mechanism of the ocean baroclinic adjustment (Nakamura *et al.* 2008), which occurs in conjunction with large sensible and latent heat fluxes on the warm side of the front (Taguchi *et al.* 2009; Nonaka *et al.* 2009) but relates it more clearly to the intermittency of atmospheric disturbances. The 48 hours needed to restore baroclinicity after a maximum of eddy heat flux is of same order as the time scale as found by Nonaka *et al.* (2009) in a composite of 8 cold air outbreaks in the Antarctic Polar Front Zone. This suggests that low-level baroclinicity is left relatively unchanged by the passage of a cyclone. Our results underpins the recent study by Papritz and Spengler (2015) showing that the steepening of isentropic slopes due to diabatic heating occurs primarily during cold air outbreaks.

Even though they did not decompose the respective contribution of latent heat release versus sensible heat flux, the presence of precipitation in the cold sector, even weak, might imply a significant contribution of the former. Indeed, as explained by Papritz and Spengler (2015), the effect of diabatic heating on isentropic slopes also depends inversely on static stability, which is relatively low in the cold sector. More work is needed to evaluate precisely the role of latent heat release in restoring baroclinicity in the cold sector.

In order to distinguish between the direct and indirect effects of the SST front on the ascent in the warm sector and to evaluate how the restoration of baroclinicity in the cold sector favours the anchoring of the storm track, new approaches need to be developed. One possibility is to apply an interactive mask in a CGCMs which would modulate air-sea fluxes in the cold and warm sectors. Such an interactive masking is under development and will be the object of another study.

Acknowledgement

B. Vannière was funded by the Natural Environment Research Council through the grant NE/J023760/1.

References

Ambaum MH, Novak L. 2014. A nonlinear oscillator describing storm track variability. *Quarterly Journal of the Royal Meteorological Society* **140**(685): 2680–2684.

Berrisford P, Dee D, Fielding K, Fuentes M, Kallberg P, Kobayashi S, Uppala S, *et al.* 2009. The era-interim archive. *ERA report series* (1): 1–16.

Brayshaw DJ, Hoskins B, Blackburn M. 2009. The basic ingredients of the north atlantic storm track. part i: Land-sea contrast and orography. *Journal of the Atmospheric Sciences* **66**(9): 2539–2558.

Chelton DB, Schlax MG, Freilich MH, Milliff RF. 2004. Satellite measurements reveal persistent small-scale features in ocean winds. *Science* **303**(5660): 978–983.

Hand R, Keenlyside N, Omrani NE, Latif M. 2014. Simulated response to inter-annual sst variations in the gulf stream region. *Climate dynamics* **42**(3-4): 715–731.

Hawcroft M, Shaffrey L, Hodges K, Dacre H. 2012. How much northern hemisphere precipitation is associated with extratropical cyclones? *Geophysical Research Letters* **39**(24).

Hoskins BJ, Valdes PJ. 1990. On the existence of storm-tracks. *Journal of the atmospheric sciences* **47**(15): 1854–1864.

Hotta D, Nakamura H. 2011. On the significance of the sensible heat supply from the ocean in the maintenance of the mean baroclinicity along storm tracks. *Journal of Climate* **24**(13): 3377–3401.

Köhler M. 2005. Improved prediction of boundary layer clouds. *ECMWF Newsletter* **104**: 18–22.

Köhler M, Ahlgrimm M, Beljaars A. 2011. Unified treatment of dry convective and stratocumulus-topped boundary layers in the ecmwf model. *Quarterly Journal of the Royal Meteorological Society* **137**(654): 43–57.

Kuwano-Yoshida A, Minobe S, Xie SP. 2010. Precipitation response to the gulf stream in an atmospheric gcm*. *Journal of Climate* **23**(13): 3676–3698.

Liu JW, Xie SP, Norris JR, Zhang SP. 2014. Low-level cloud response to the gulf stream front in winter using calipso*. *Journal of Climate* **27**(12): 4421–4432.

Minobe S, Kuwano-Yoshida A, Komori N, Xie SP, Small RJ. 2008. Influence of the gulf stream on the troposphere. *Nature* **452**(7184): 206–209.

Minobe S, Miyashita M, Kuwano-Yoshida A, Tokinaga H, Xie SP. 2010. Atmospheric response to the gulf stream: seasonal variations*. *Journal of Climate* **23**(13): 3699–3719.

Nakamura H, Sampe T, Goto A, Ohfuchi W, Xie SP. 2008. On the importance of midlatitude oceanic frontal zones for the mean state and dominant variability in the tropospheric circulation. *Geophysical Research Letters* **35**(15).

Nonaka M, Nakamura H, Taguchi B, Komori N, Kuwano-Yoshida A, Takaya K. 2009. Air-sea heat exchanges characteristic of a prominent midlatitude oceanic front in the south indian ocean as simulated in a high-resolution coupled gcm. *Journal of Climate* **22**(24): 6515–6535.

Papritz L, Spengler T. 2015. Analysis of the slope of isentropic surfaces and its tendencies over the north atlantic. *Quarterly Journal of the Royal Meteorological Society* .

Parfitt R, Czaja A. 2015. On the contribution of synoptic transients to the mean atmospheric state in the gulf stream region. *Quarterly Journal of the Royal Meteorological Society* .

Pfahl S, Madonna E, Boettcher M, Joos H, Wernli H. 2014. Warm conveyor belts in the era-interim dataset (1979–2010). part ii: Moisture origin and relevance for precipitation. *Journal of Climate* **27**(1): 27–40.

Small R, Xie S, ONeill L, Seo H, Song Q, Cornillon P, Spall M, Minobe S, *et al.* 2008. Air-sea interaction over ocean fronts and eddies. *Dynamics of Atmospheres and Oceans* **45**(3): 274–319.

Taguchi B, Nakamura H, Nonaka M, Xie SP. 2009. Influences of the kuroshio/oyashio extensions on air-sea heat exchanges and storm-track activity as revealed in regional atmospheric model simulations for the 2003/04 cold season*. *Journal of Climate* **22**(24): 6536–6560.

Vanniere B, Czaja A, Dace H, Woollings T. 2015. Gulf stream-troposphere connection : the ”cold path”. *Journal of Climate* .

Vannière B, Czaja A, Dacre H, Woollings T, Parfitt R. 2015. A potential vorticity signature for the cold sector of extratropical cyclones. *Submitted to QJRMS* .

Vannière B, Czaja A, Dacre H, Woollings T, Parfitt R. 2015. A potential vorticity signature for the cold sector of winter extratropical cyclones. *Quarterly Journal of the Royal Meteorological Society* .

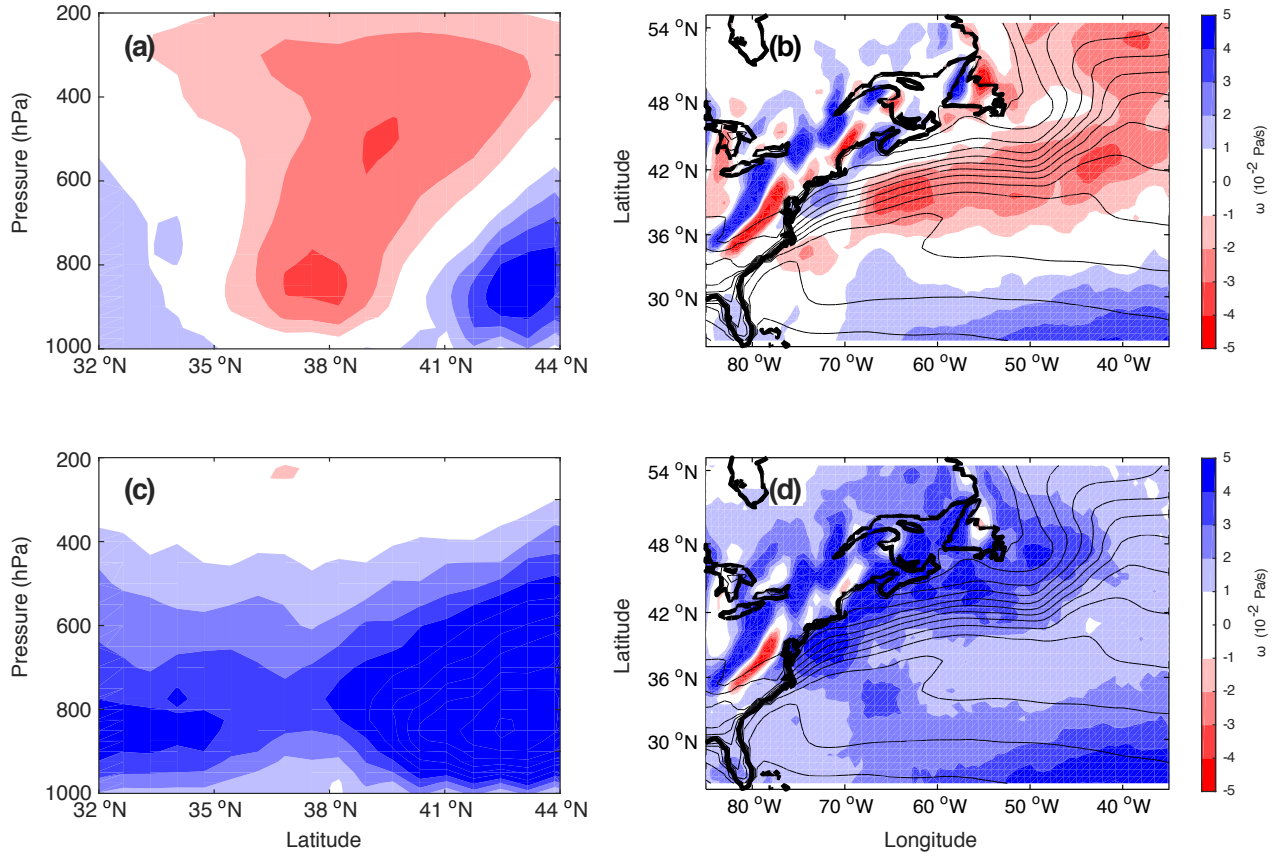

Figure 1. DJF statistics pressure vertical velocity (ω in Pa/s) in the ERA-interim reanalysis dataset averaged over the 1979-2010 period. Latitude - pressure section at $60^{\circ}W$ for (a) the mean and (c) the median of ω Longitude - latitude sections at 500hPa for (b) the mean and (d) the median of ω. SST (black contours every 2K).

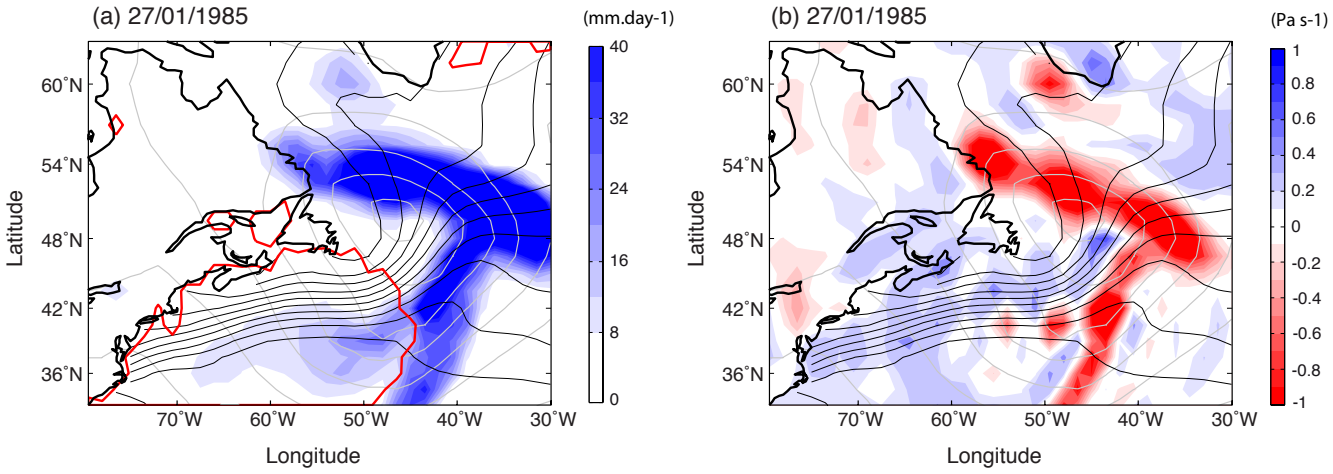

Figure 2. Case of an extratropical cyclone over the Gulf Stream region at 0000 UTC on 27/01/1984 (a) total precipitation (blue), sea-level pressure (grey contours, every 5mb), SST (black contours, every 2K) and red contours (1_{CS}); (b) same (a) but shadings represent vertical velocity in pressure coordinates at 700 mb (Pas^{-1}).

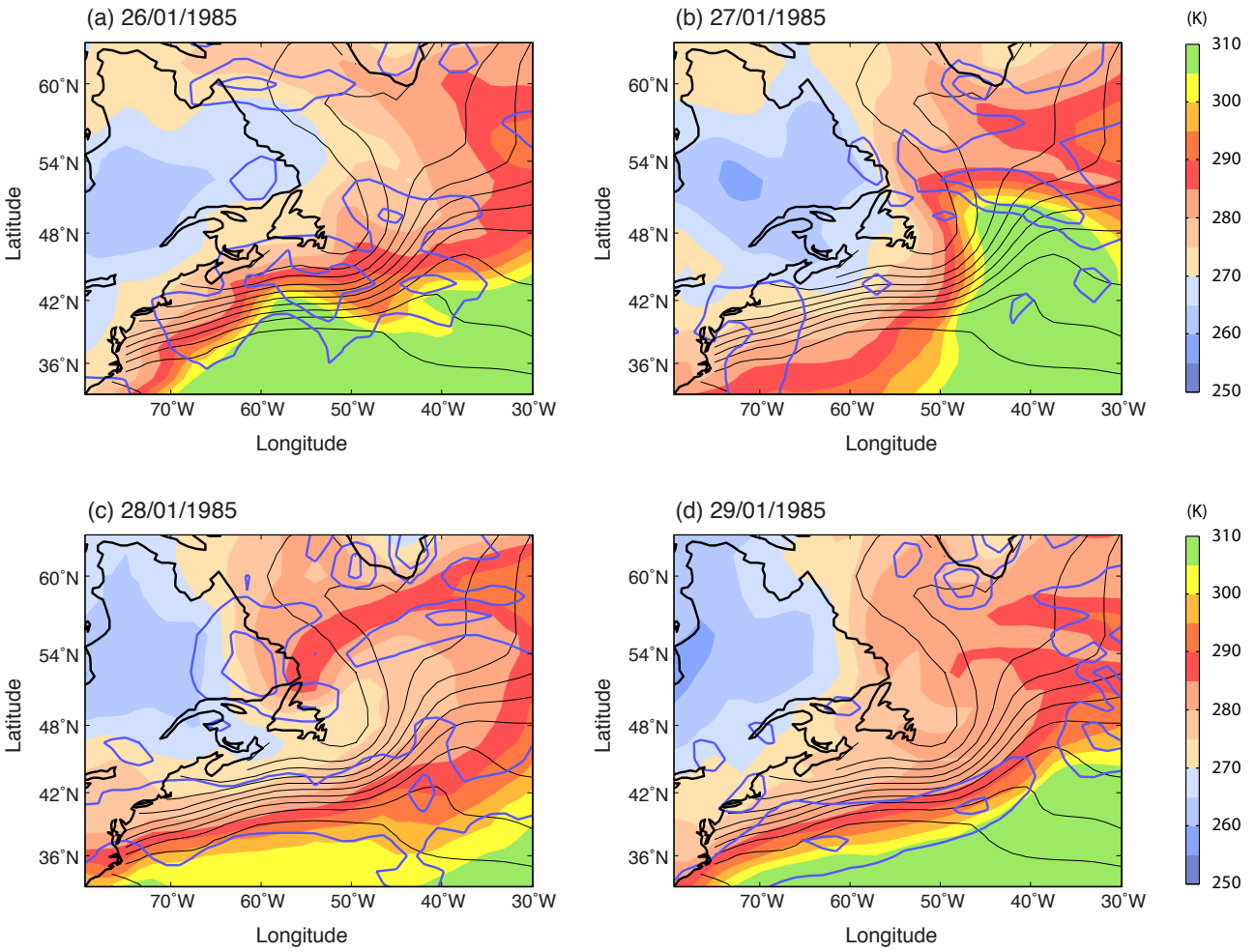

Figure 3. Evolution of equivalent potential temperature (color shadings), the Eady parameter (blue contours, every 1 day^{-1}) and SST (black contours, every 2K) at 0000UTC (a) on 26 January, (b) on 27 January when the extratropical cyclone reaches its maximum intensity, (c) on 28 January and (d) on 29 January.

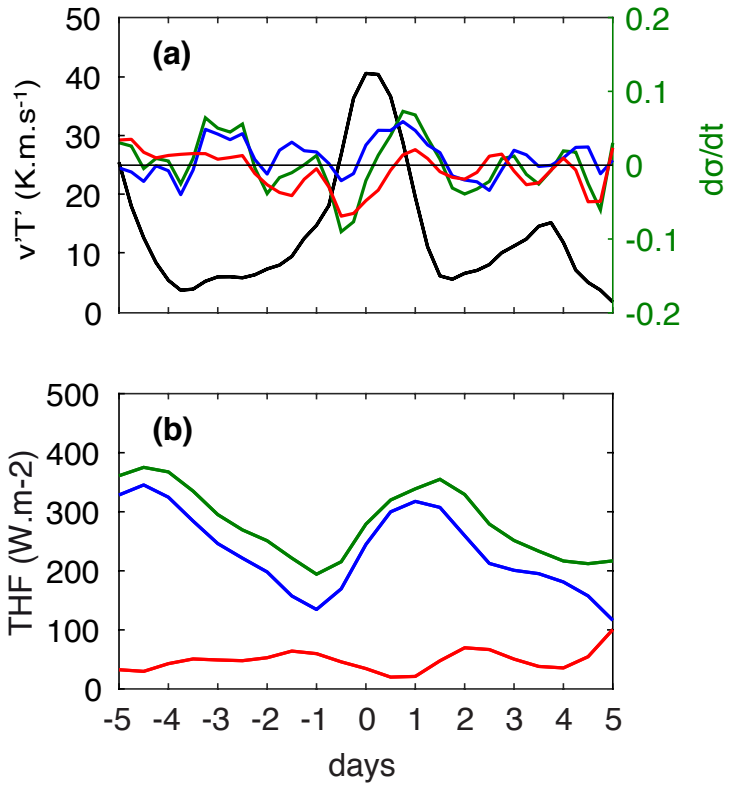

Figure 4. Evolution from 22 January 1985 to 1 February 1985 of (a) eddy heat flux at 850 mb (black curve), tendency of baroclinicity at 775 mb (green curve in $day^{-1}(6hours)^{-1}$), contribution of cold sector situations to tendency of baroclinicity, i.e. $\mu_{CS}(\sigma)$, (blue curve) and contribution of non cold sector situations, i.e. $\mu_{\overline{CS}}(\sigma)$ (red curve); (b) total heat flux (green), contribution of cold sector situations to total heat flux, i.e. $\mu_{CS}(THF)$, (blue curve) and contribution of non cold sector situations, i.e. $\mu_{\overline{CS}}(THF)$, (red curve). All quantities are averaged over the domain [80°W-30°W,30°N-50°N].

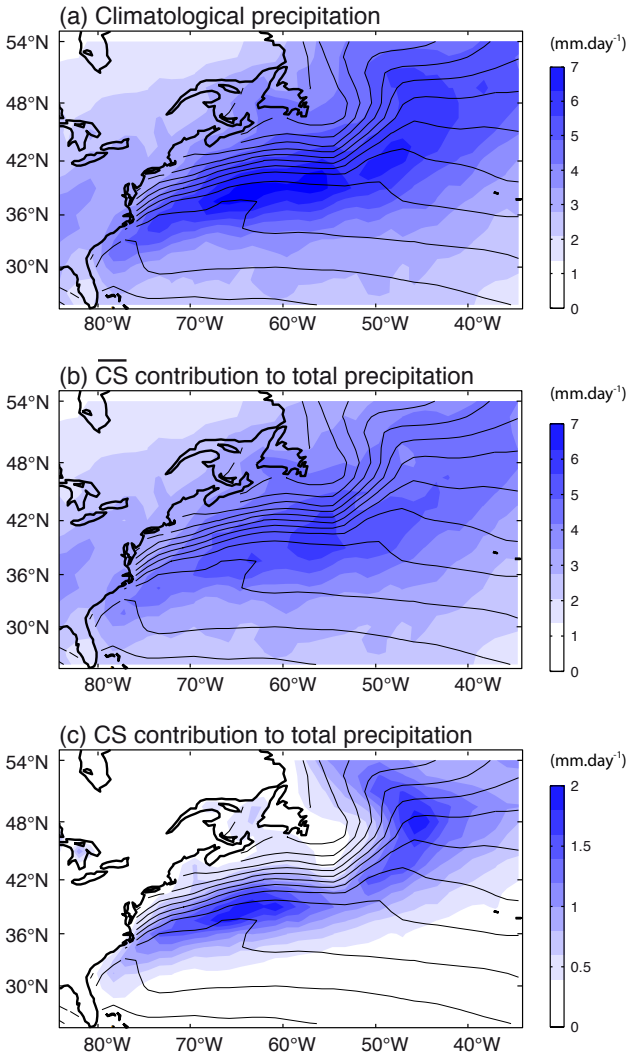

Figure 5. ERA interim precipitation (mm/day^{-1}) (a) climatological mean, (b) contribution to climatological mean precipitation from outside the cold sector ($\mu_{\overline{CS}}(P)$), (c) contribution to climatological mean precipitation from the cold sector ($\mu_{CS}(P)$).

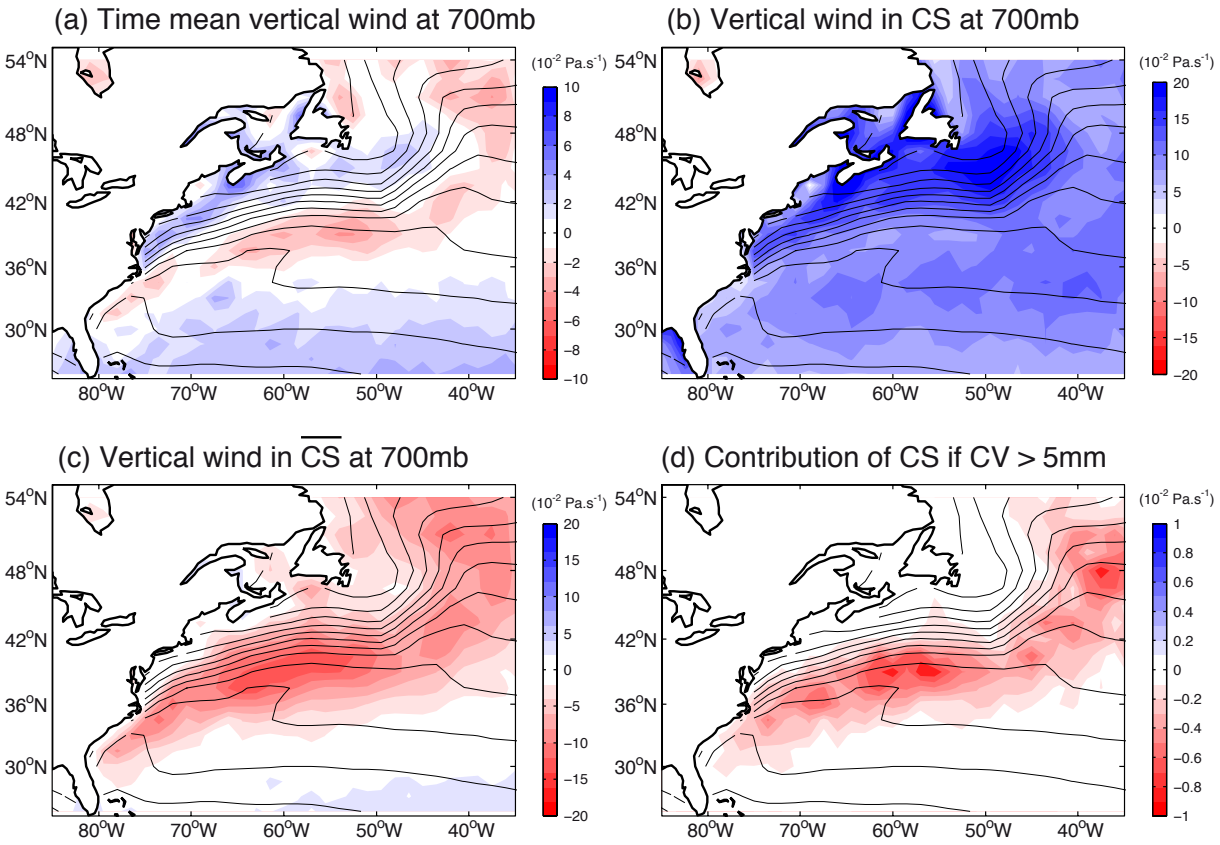

Figure 6. Vertical wind in pressure coordinates at 700 mb ($Pa.s^{-1}$): (a) climatological mean, (b) mean of the cold sector situations, i.e. $m_{CS}(\omega_{700})$, (c) mean of non cold sector situations, i.e. $m_{\overline{CS}}(\omega_{700})$, (d) contribution of cold sector to total wind when convective precipitation is above 5 $mm.day^{-1}$, i.e. $\mu_{CS}(\omega_{700})$ when convective precipitation is larger than 5 mm.day^{-1}

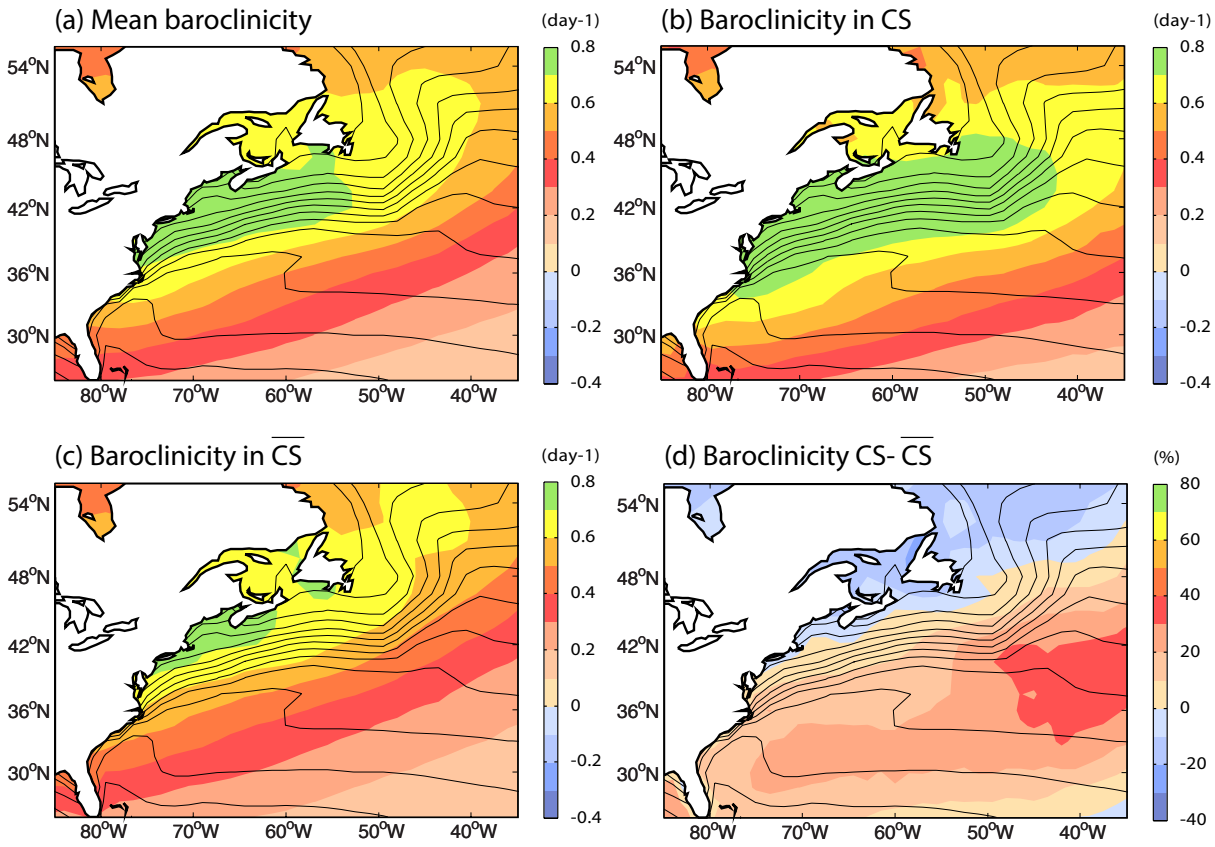

Figure 7. Eady parameter (day^{-1}): (a) climatological mean, (b) mean of the cold sector situations, i.e. $m_{CS}(\sigma)$, (c) mean of non cold sector situations, i.e. $m_{\overline{CS}}(\sigma)$. (d) Percentage change of Eady parameter between CS and $\overline{CS}$, i.e. between $m_{CS}(\sigma)$ and $m_{\overline{CS}}(\sigma)$.

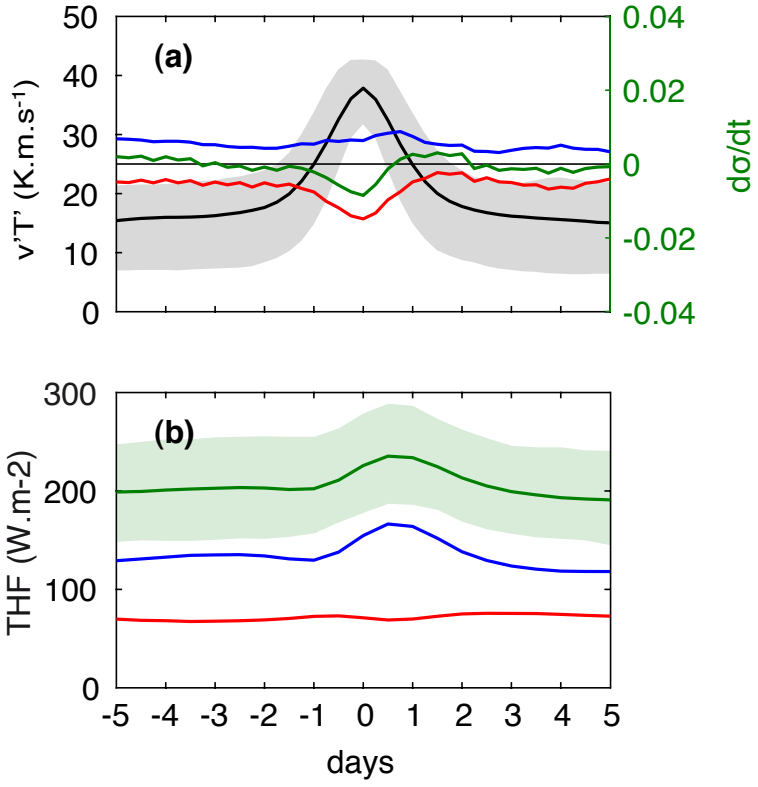

Figure 8. Composite around time maxima of horizontal eddy heat fluxes at 850 mb; (a) eddy heat flux (black curve) and its interquartile range (black shadings), tendency of baroclinicity at 775 mb (green curve, in $day^{-1}(6hours)^{-1}$) and its interquartile range (green shadings), contribution of cold sector situations to tendency of baroclinicity, i.e. $\mu_{CS}(\sigma)$, (blue curve) and contribution of non cold sector situations, i.e. $\mu_{\overline{CS}}(\sigma)$ (red curve); (b) total heat flux (green) and its interquartile range (green shadings), contribution of cold sector situations to total heat flux, i.e. $\mu_{CS}(THF)$, (blue curve) and contribution of non cold sector situations, i.e. $\mu_{\overline{CS}}(THF)$, (red curve). All quantities are averaged over the domain [80°W-30°W,30°N-50°N].

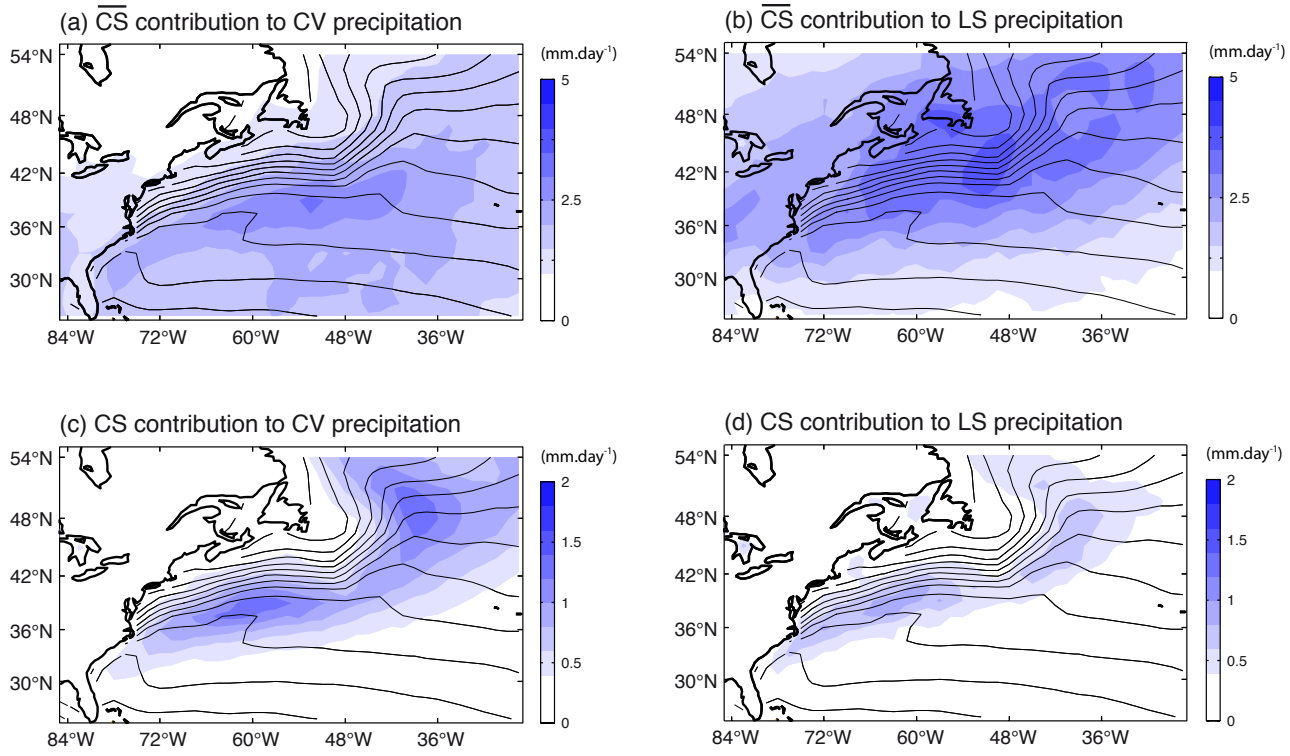

Supplementary figure 9. Supplementary. ERA interim precipitation decomposed as precipitation in convective (a,c) and large scale (b,d) occurring in $\overline{CS}$ (a,b) and CS (c,d).